









Improvement of thermal stability and gamma-ray absorption in microwave absorbable poly(methyl methacrylate)/graphene nanoplatelets nanocomposite

Tayfun Bel¹  | Mahmut Muhammettursun¹  | Elif Kocacinar¹  |
 Ecem Erman¹  | Fuat Berke Gul¹  | Emre Dogan²  | Murat Celep³  |
 Nilgun Baydogan¹ 

¹Istanbul Technical University, Energy Institute, Ayazaga Campus, Istanbul, Turkey

²Physics Department, Bursa Uludag University, Bursa, Turkey

³TUBITAK, National Metrology Institute, Gebze Campus, Gebze, Turkey

Correspondence

Nilgun Baydogan, Istanbul Technical University, Energy Institute, Ayazaga Campus, Istanbul, Turkey.
 Email: dogannil@itu.edu.tr

Funding information

Istanbul Teknik Üniversitesi, Grant/Award Number: 41576; TUBITAK, Grant/Award Number: TUBITAK1001 115R017

Abstract

The graphene nanofiller (2 wt%) was dispersed in poly(methyl methacrylate) by in situ polymerization method. The optimum high frequency (microwave) absorption was evaluated at X-band due to changes in the scattering parameters (determined by using a vector network analyzer). The slight improvement has been attained in gamma attenuation coefficient of the polymer nanocomposite by using gamma transmission technique. The addition of graphene nanoplatelets (2 wt%) resulted in a thermal improvement from 196.73 to 243.00°C (with 5% weight loss) in TGA analysis. The graphene nanoplatelets provided an optimum decrease in scattering of the microwaves due to the elimination of the defects and the prevention of the agglomeration of the graphene nanoplates. The improvement of microwave absorption (between 8 and 12 GHz) suggested that the nanocomposite was a suitable candidate as a microwave absorbing material. This multipurpose nanocomposite has provided thermal stability and it has ensured the optimum gamma-ray and microwave absorption depending on the development of the structural properties. The development of these physical characteristics has enabled to improve the electrical conductivity as a result of the progress in the structural properties.

KEYWORDS

applications, synthesis and processing techniques, thermoplastics

1 | INTRODUCTION

The broadband wireless communication systems require the use of sophisticated materials to enable reliable long-range communication with high sensitivity. The absorption-based protective screening materials can be used in radar and microwave communication technologies to achieve good absorption with a wide bandwidth (such as X-band). The cost-effective production of the

radar wave absorber can be obtained by the limitation of reflection loss at the absorption-based lightweight screening materials (such as the modified polymer composites).¹ The potential satellite-oriented polymer materials require resistant to gamma ray transmission in the extreme space environment at outer ring of Van Allen Belts.² Poly(methyl methacrylate) (PMMA) can be used at lighting and sanitary components. The users in many application areas are demanding technical improvements

of PMMA. But the properties of PMMA need to be improved with nanofillers^{2,3} as it has lack suitable physical properties for high-tech applications.^{4,5} The large range of transition metal catalyst list (such as ruthenium, copper, nickel, iron, palladium, and rhodium) is available for the synthesis of PMMA by using atom transfer radical polymerization (ATRP) method. Copper-based transition metal catalyst is useful to synthesis the cross-linkable PMMA derived from MMA (with the easy polymerizable property).^{6–9} PMMA can be carried out to avoid the formation of the optimum reflectance which is the received signal with a nominal bandwidth of 70 GHz.⁸ The use of graphene presents the optimum bandwidth covers the X-band applications.^{10–15} Nano and micro-size particles are used to improve the physical properties of PMMA.^{9,16} The addition of graphene nanoplatelets (GNPs) into a polymer nanocomposite enables the improvement of the poor physical properties of the polymer.^{10–15} The maximum structural improvement is obtained at a lower GNPs concentration such as 0.3 and 1 wt% in literature.^{9,12,16} The deterioration in structural properties (with lower improvements in thermal stability) can be the results of the cracks and pores⁹ or agglomeration of GNPs in the composite matrix.^{10,12–21} The details about the decrease of the scattering of the microwave absorbance at X band are not available for the synthesis of PMMA/GNP nanocomposite (based on the result of the elimination of the structural defects and the agglomerations) by using ATRP method in literature. Aggregates can cause to the decrease the dispersion of nanofiller at high concentrations.¹⁷ Agglomeration in GNP composites results with the stacking of flaky-shaped GNP particles.¹⁸ The strong tendency of GNP aggregation causes problems such as the difficulty in exfoliating GNP in the polymer.

The crack can be appeared at carbon nanotubes with increasing sonication time and carbon nanotubes can disintegrate into smaller size particles above 40 min of sonication time. The increase of the aggregation of carbon nanotubes in the dispersion affects the thermal properties due to smaller size particles.²² The nanomaterial presents a considerable dispersion problem in matrix owing to its high specific surface area.²³ Besides, the sharp edges of GNP can cause the density changes to initiate lower physical properties.¹⁸ The lower interaction between GNP filler and PMMA affects the thermal properties of the nanocomposite.^{24,25} Hence it is assumed that it is important not to use the magnetic stirrer that the mixing process can create the damage at GNP in this study.

ATRP method enables excellent control on the polymer molecular weight, polydispersity index, composition and end-group functionality.^{10,12,13} The improvements of interface between graphene flakes and PMMA composites can be performed avoiding the non-crack surface of nanocomposite.²⁶ The strong interface between GNS and

polymer is crucial to achieve high thermal performance at the polymer nanocomposite.^{27,28} The enhancement in thermal resistance depends on the higher thermal stability of graphene.²⁸ The decrease in diffusion (with the migration of volatile molecules from the inside of the matrix to the surface) causes the higher degradation temperatures.²⁷ There are not considerable details about the suitable GNPs amount in PMMA to make an optimization at the dispersion considering the thermal stability of the PMMA/GNPs nanocomposite derived by the ATRP method. The controlled/living polymerization technique can provide the controlled molecular weight and distribution considering PMMA/GNP nanocomposite so that the chain growth is possible in this study (according to literature).^{19,20}

The sharp edges of GNP at the stacking event initiated to decrease the protective gamma absorption as the sharp edges caused to initiate the cracks at the nanocomposite in this study. The uses of gamma transmission technique (based on the calculation of gamma-ray attenuation at the nanocomposite) provided the determination of the dispersion to avoid the agglomeration. The sensitive control of the sharp edges effect by using gamma transmission technique provided to eliminate the cracks at the optimum GNP amount in the nanocomposite. The application of this technique has supported to make the limit of the serious absorption mechanism problems for microwave attenuation by means of tuneable range control at X-band. Hence the solution of the technical architecture needs has provided the removal of conductivity problems to initiate the developments in the new nano-compatible polymer in IoNT applications by using GNPs. The results of this study indicated that the solution of the technical problems of the non-crack structure with the optimum thermal performance has improved the working conditions of the nanocomposite in aggressive environments due to the derived gamma-ray absorption and the optimum microwave absorbability. This conductive PMMA/GNPs nanocomposite indicates to enhance this innovative conductive bulk polymer adaptation for its use in Internet of Nano Things (IoNT) systems. The structural development has explained the innovative relation between gamma-ray attenuation enhancement and thermal stability development with the improvement of the electrical conductivity in this lightweight nanocomposite.

2 | EXPERIMENTS

2.1 | Preparation of PMMA/GNP nanocomposite

Tetra-*n*-butylammonium bromide (Bu₄NBr; 98 + %; Alfa Aesar), Copper (I) bromide (CuBr; Puratronic®, 99.998%;

metals basis; Alfa Aesar), methyl methacrylate (MMA; 99%, stabilized; Alfa Aesar), and 1,1,4,7,7-pentamethyldiethylenetriamine (PMDETA; 98%; Alfa Aesar), ethyl 2-bromoisobutyrate (EBiB; 98 + %; Alfa Aesar) were used for the preparation of the polymer solution. Bu_4NBr (1.211 g, 3.76 mmol) and CuBr (0.067 g, 0.47 mmol) was prepared for the synthesis of the polymer nanocomposite. The used GNP (99.5 + %, Nanografi) had a surface area of $150 \text{ m}^2/\text{g}$, thickness of 6 nm, and surface diameter of $5 \mu\text{m}$. CuBr as the catalyst was used at ATRP method because of its higher synthetic efficiency, its economic and practical process.

GNP (with four different amounts: 0.25, 0.5, 1, and 2 wt%) was added to the borosilicate tubes ($8 \times 2.5 \text{ cm}^2$) equipped inside AtmosBag in argon. The previously prepared monomer MMA (28.2 g, 0.282 mol) was added to each tube using a gas tight syringe; then, the ligand PMDETA (0.081 g, 0.47 mmol) was added to the tubes and premixed for 15 min using a rotating shaker. The mixture was degassed severely through glass frit with pure argon for 5 min. Then, EBiB (0.092 g, 0.47 mmol) was added to the tubes, and the tube was sealed with a rubber septum followed by parafilm sealing. Then the mixture has been stirred by using the rotating shaker. The schematic diagram of interaction of graphene nanoplatelets filler and PMMA was presented in Figure 1. The tube was put on the rotating shaker (suitable for continuous running with speed range at 30 rpm) to avoid the cracking of GNP in the polymer solution as the magnetic stirring bars could cause damage. The GNP nanofiller at four different amounts (such as 0.25, 0.50, 1.00, and 2.00 wt%) was dispersed via in situ polymerization.

2.2 | Structural characterization

XRF analysis was conducted by using Olympus Innov-X XRF analyzer to examine the copper amount of the base PMMA and PMMA/GNP nanocomposite at 2 wt% GNP (in Table 1).

The characterization of the PMMA/GNP nanocomposite samples was carried out with different GNP amount by using the FEI-Quanta FEG 250 Model scanning electron microscope (SEM).

TGA analysis was performed by using a TA Instrument Standard Dual Instrument. The measurements were taken over a temperature range from room temperature (25°C) to 600°C with the heating rate of 20°C per minute. 5 mg sample was placed in a platinum pan and put into the insulated furnace. TGA analysis was performed in nitrogen. The electrical resistivity of the surface of the PMMA/GNPs nanocomposites was measured by using four-point probe (SIGNATONE) Keithley 2000 source meter.

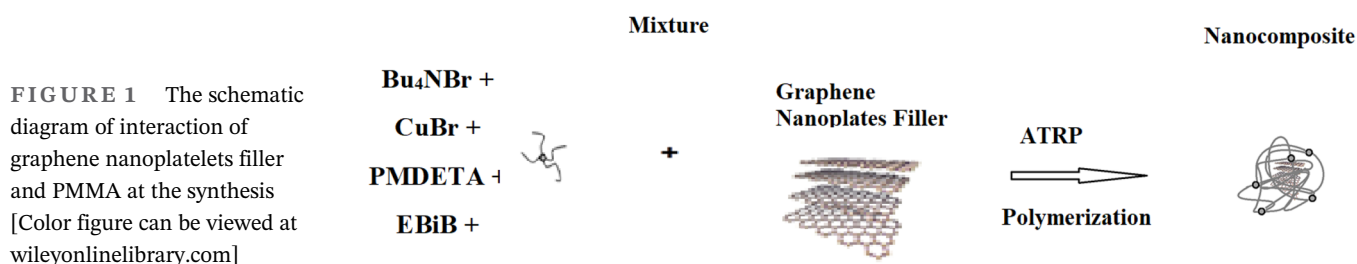
A Perkin Elmer Spectrum 100 FTIR spectrometer (connected to the computer) was used to analyze the samples. Thermo K-Alpha X-ray Photoelectron Spectroscopy (XPS) was used to analyze the surface chemistry of the samples as this technique was highly surface sensitive (with the detection depth $\sim 5 \text{ nm}$). Dry solid samples were used at XPS analysis.

2.3 | Application of gamma transmission technique

The effects of the gamma attenuation coefficient on PMMA/GNP nanocomposites were analyzed with increasing GNP concentration by using two gamma radioisotopes. For this purpose, Cs-137 and Co-60 radioisotopes were selected as gamma sources to investigate the attenuation coefficients of the PMMA/GNP nanocomposites. The Cs-137 radioisotope has a gamma peak at 0.662 MeV (a 30.1-year half-life) and the Co-60 gamma radioisotope has two gamma peaks at 1.17 and 133 MeV (with 5.23 years half-life). The average energy value of two gamma peaks of Co-60 is accepted as a monochromatic energy having $\sim 1.25 \text{ MeV}$. Because, the communication satellites service at the extreme ionizing radiation region of space environment consists of two

TABLE 1 XRF analysis results about copper in base PMMA and PMMA/GNP nanocomposite

Cu	ppm	+/-
Base PMMA	4502	71
PMMA/GNP at 2 wt% GNP	4205	62



radiation rings named Van Allen belts (which are in the form of two radiation rings) around the Earth. Hence, the communication satellites require to achieve optimum wide bandwidth (such as in X-Band) absorption in the harsh radiation environment. The outer ring comprises of lighter particles (such as the trapped high energy electrons and positrons in the Earth's magnetic field). The inner ring contains highly energetic protons (with energy exceeding 30 MeV) affected from the gravity force as the mass of protons are considerably higher than that of the positrons. Electrons moving at speeds close to the speed of light in the outer belt pose a danger for the telecommunication satellites at the service area in Earth orbit. The Coulomb Forces constitute the major mechanism of energy loss for electrons (for either positive or negative charge). The impulse and energy transfer to space material are about the same for the electrons (with a positive or negative charge). The photons emission generated by the bremsstrahlung event as the electrons (with a positive or negative charge) is accelerated around the nucleus of the ionized atom in the material due to Coulomb Forces. When the electrons (with a positive or negative charge) is accelerated around the lightweight atom of the space material (such as the modified polymer), the radiation with a slight intensity is emitted. Hence the use of lightweight material is important to avoid intense bremsstrahlung radiation in space material applications.²⁵ The positron (which is an electron with an electric charge of +1) interact similarly with the polymer nanocomposite when it is energetic. But, the behavior of positron differs from the electron with the negative charge at the end of its path in the material. When a positron (antimatter particle) comes to rest, it interacts with an electron of the atom. The positron is released by positron decay event and annihilation reaction produces two energetic photons with 511 keV energy (which is close to Cs-137 radioisotope's gamma peak at 0.662 MeV). Hence, the threat of the outer radiation ring requires the development of the lack of physical properties of polymers to protecting satellites critical infrastructure. Commercial satellites have to be modified against the rigors of space like radiation and debris. The bremsstrahlung from high-energy electrons in the atomic field of the material used in the device can be vulnerable for the satellites as blocking communication between a satellite and the ground. The bremsstrahlung photons and annihilation radiation (generated by the positrons) can cause to disrupt a satellite's normal operations or to destroy a satellite by creating an unsuitable electronic signal that could cause it to tumble from its orbit. The outside of the devices (such as the synthesized signal generators) can become even lighter by using lightweight material such as a polymer. The outer box in the device used in commercial satellites to

fulfill its communications and information transmission requirements generates the signal. The outside of the outer box at the device (such as the synthesized signal generator) is more exposed to the outside environment and therefore its electromagnetically working conditions are heavier. The inner side of the box including a polymer is relatively less exposed to the space radiation.

The gamma source and detector were placed face-to-face on the same axis. The gamma spectrometer was used to measure the linear attenuation coefficients of the samples. It contains a detector (Canberra Bicron Model: 802-2X2) and is connected to a 1024-channel Multi-Channel Analyzer. The diameters of the Cs-137 and Co-60 radioisotopes were 6 mm, while the hole of the lead collimator had a diameter of 7 mm. The diameter of the detector was 20 mm, and the thickness of the lead collimator was 10 mm. A distance of 187 mm was maintained between the radiation source and the detector during the measurements. The detector has recorded the gamma ray intensity from the source and the initial baseline intensity (I_0) was recorded without using the composite material at the beginning of the measurement. The PMMA/GNP nanocomposites were placed between the gamma source and the detector and then the transmitted gamma rays (I) from the nanocomposite was determined with the rise of the PMMA/GNP nanocomposites thickness. The distance between the radiation source and the composite material was 140 mm. All of the measurements were performed at least five times with the same measurement parameters.

2.4 | Microwave measurements

A vector network analyzer (VNA; R&S ZVA), VNA cables, related adapters and X-band calibration kit were used to measure the scattering (S) parameters of the PMMA/GNP polymer nanocomposite. A reference plane for port 1 and port 2 of the VNA included cables. The waveguide adapters were defined at connection points of the PMMA/GNP polymer nanocomposite. The VNA was calibrated with short, offset-short and load technique using the X-band calibration kit at the reference planes.

The PMMA/GNP nanocomposite with 2 wt% GNP concentration was prepared with 22.86 mm length, 10.16 mm high, and 9.78 mm thickness using the $\frac{1}{4}$ Wavelength Shim (in Figure 2(a)). The PMMA/GNP nanocomposite was put into the $\frac{1}{4}$ Wavelength Shim made of aluminium (the aluminium purity was at 99.3%) in Figure 2(b). The specifications about the properties of the $\frac{1}{4}$ Wavelength Shim were presented to explain the details about the S-parameters of microwaves at the PMMA/GNP nanocomposite in Figure 2(c). The

FIGURE 2 (a) Prepared PMMA/GNP polymer nanocomposite on $\frac{1}{4}$ wavelength shim made of aluminium, (b) the placement of the nanocomposite into the $\frac{1}{4}$ wavelength shims, and (c) the schematic illustration of the prepared shim with special sizes [Color figure can be viewed at wileyonlinelibrary.com]

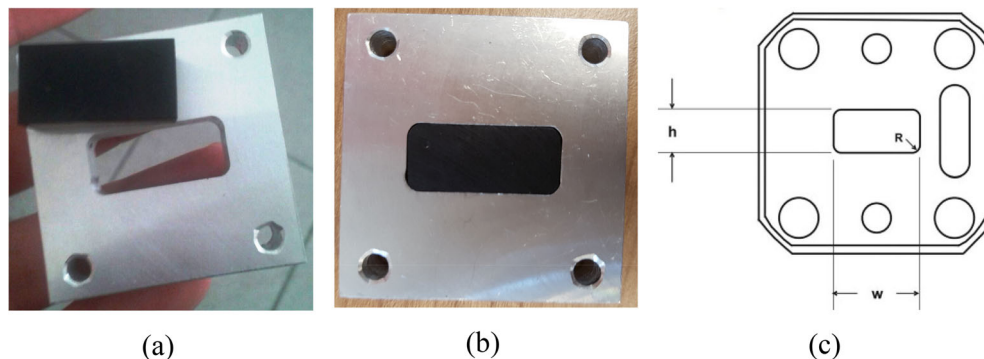


TABLE 2 Dimensions of the $\frac{1}{4}$ wavelength shim

Frequency band (GHz)	Waveguide band	w (mm)	h (mm)	R (mm)	Thickness (mm)
8.2–12.4	WR90	22.86 ± 0.01	10.16 ± 0.01	0.13 max.	9.78 ± 0.02

details about the size of shim were presented in Table 2. The S-parameters of the PMMA/GNP polymer nanocomposite were measured using calibrated VNA.

3 | RESULTS AND DISCUSSION

The surface morphologies of (a) GNP, (b) pure PMMA and PMMA/GNP nanocomposite samples in (c) 0.25 (d) 2 wt% GNPs amount were presented at FESEM images in Figure 3. For the mixing of the solution with suitable fluidity, the optimum conditions have been obtained during stirring by using the rotating shaker in Figure 3(c,d). The surface morphology of base PMMA was relatively flat and smooth than nanocomposite at low GNS content (0.25 and 2 wt% GNP amount) in this study. The surfaces of PMMA/GNP nanocomposite samples indicate that the GNP was dispersed in the nanocomposite (in Figure 3(c,d)). As the suitable fluidity with the spread of the MMA monomers have been obtained during stirring the polymerization of the monomer has resulted with the optimum interaction between GNP and PMMA at the PMMA/GNP nanocomposites in Figure 3(c,d). The obvious cracks and pores or significant agglomeration were not observed in the nanocomposite at GNP (2 wt%). It was suggested that this non-crack structure was a suitable lightweight shielding material candidate. It was possible to avoid the gamma- efflux from fractured sites and it was obtained to prevent the efflux of microwave from cracks or pores. It was assumed that the argon ambient was important as the use of an inert atmosphere at the preparation of the polymer solution to improve the physical properties such as electrical performance and thermal resistance as the result of the non-cracked morphology. SEM images indicated that

the synthesized nanocomposite samples had the obvious non-fractured surfaces. Hence it was assumed that they have the special surfaces to obtain the optimum gamma attenuation coefficient and they were suitable to use them at the cost-effective radar absorbing applications.

For pure PMMA, the elemental mapping is presented for C atoms in Figure 4(a) and the elemental mapping of Cu atoms is available in Figure 4(b). The elemental mapping for C atoms (in Figure 4(c)) and for Cu atoms (in Figure 4(d)) were submitted in the PMMA/GNP nanocomposite at 2.0 wt% GNP concentration.

Figure 5 has presented the TGA curves of PMMA and PMMA/GNPs nanocomposites. The changes in temperature at 5% weight loss of PMMA and PMMA/GNPs nanocomposite were given in Table 3. The addition of GNPs (at 0.25wt) supported to increase the 5% weight loss temperature of the pure PMMA by 22.6°C. The 5% weight loss temperature of PMMA/GNPs nanocomposite (with 2 wt% GNPs) shifted from 197 to 243°C with an improvement on 46.27°C. The addition of GNPs nanofiller into the PMMA resulted with the improvement in the thermal stability of the PMMA/GNPs nanocomposite (in Figure 5(a)). The thermal degradation of the PMMA/GNPs nanocomposite was shifted to higher temperatures and the presence of GNPs has enhanced the thermal stability of PMMA. Some details about the addition of the CuBr by ATPP method are available (due to its higher synthetic efficiency, lower cost and a simpler process) that is compared with the thermal stability of the PMMA/GNPs nanocomposite in the literature.²⁹ FTIR analysis results were presented at 0.2, 0.5, 1, 1.5, 2, 3, and 5 wt% GNP amounts in Figure 5(b) and the similar changes of the main three peaks were obtained at the previous study.²⁹ Besides, some details about the relationship between the molecular weight and its importance

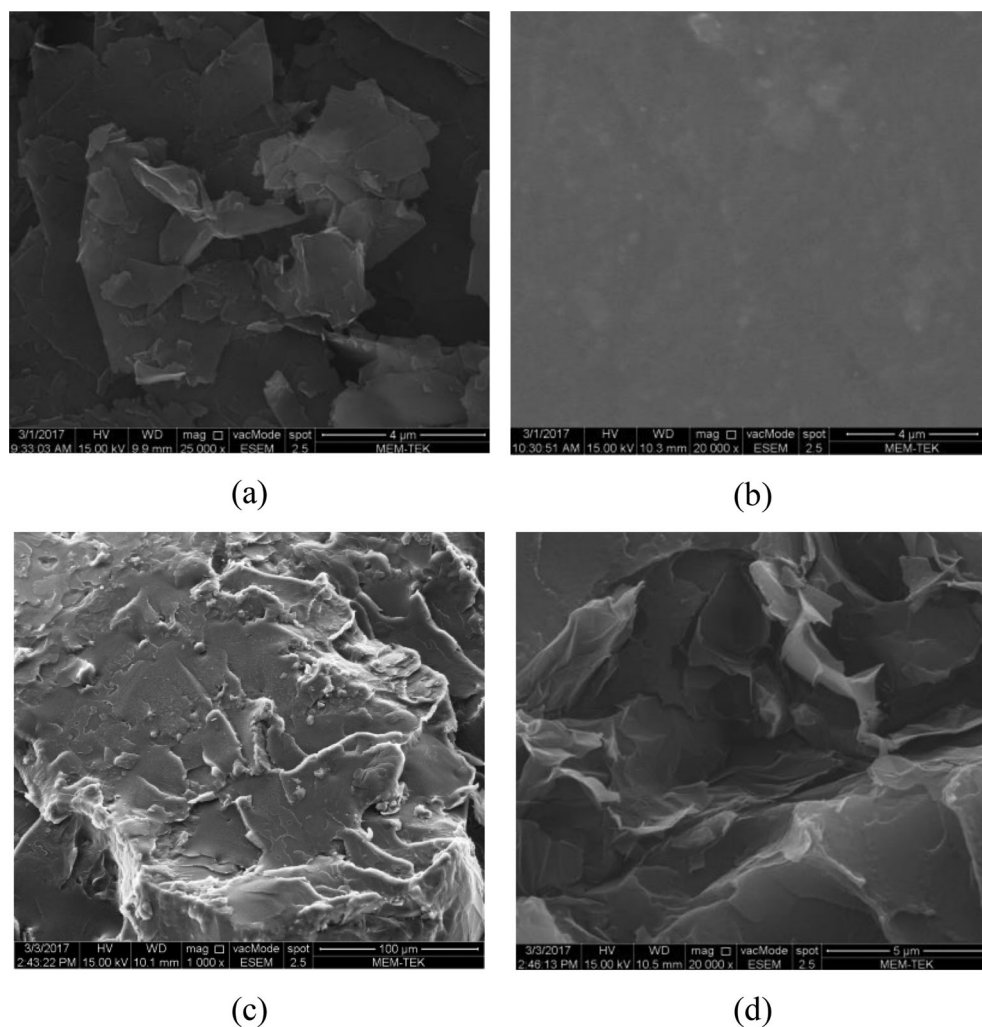


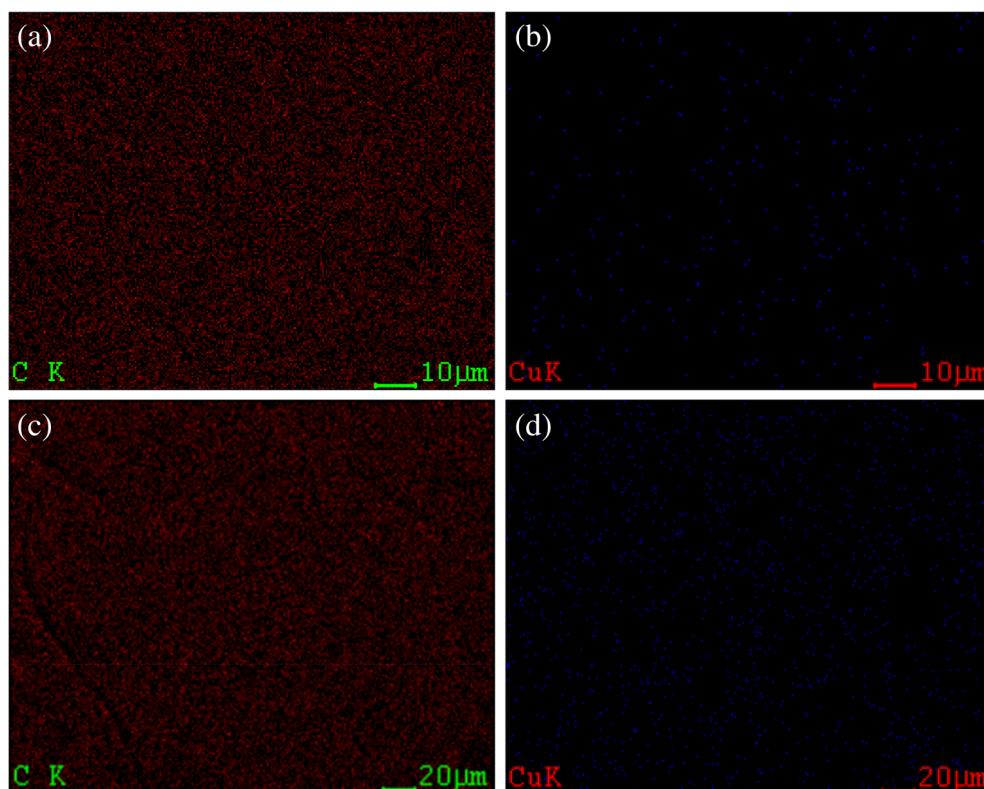
FIGURE 3 SEM images of (a) GNP, (b) pure PMMA, (c) PMMA/GNP nanocomposites with 0.25 wt%, and (d) PMMA/GNP nanocomposites with 2 wt% GNP concentrations

for its structural improvement are presented in the previous studies.^{29,30} ATRP technique enables the suitable control of the molecular weight of the polymer, polydispersity index and end-group functionality through the addition of graphene nanoparticles.²⁹ The ATRP functional groups are more suitable than other radical polymerization methods (such as ionic polymerization). Copper (I) bromide (CuBr) can be used as the catalyst. Because the use of CuBr supports higher synthetic efficiency, lower cost, and a simpler process than other catalysts. Besides, there are several advantages of this reaction such as the use of readily available starting materials and optimal product yields. ATRP method can provide to produce a satisfactory mechanical improvement with low density and optimum thickness.²⁹ Hence ATRP method is used as the suitable dispersion method for the GNP in the polymer solution as copper is one of the needful elements for the improvement of gamma-ray and microwave adsorption at ATRP method (used CuBr). The improvement of gamma-ray and microwave adsorption was examined at the PMMA/GNP nanocomposite

(having enhanced mechanical performance with low density and optimum thickness) in this study. Because the high mechanical performance is one of the important key parameters for the prolonged service life of the nanocomposite during its duty in the area. Hence the comparison about gamma-ray and microwave adsorption of the nanocomposite was performed without containing copper for the evaluation of gamma-ray and microwave adsorption in this study.

XPS survey spectra was used to characterize the change of the chemical composition of the nanocomposite in Figure 6 and their results exhibited C1s and O1s peaks. The intensity of the peaks increased with the rise of GNPs amount in PMMA. Q1s peak indicated the changes of oxygen atoms existence in the C—O and C=O functional groups and C1s spectrum addressed to the variations of the existence of C—O—C and O—C=O functional groups with the rise of GNPs amount. C1s peak centered ~285 eV and O1s placed 533 eV for GNPs/PMMA nanocomposite samples. The positions of these peaks in this study were similar with the positions of the

FIGURE 4 Elemental mapping results of pure PMMA (a) C atoms, (b) Cu atoms and elemental mapping results of PMMA/GNP with 2.0 wt% GNP amount (c) C atoms, (d) Cu atoms for PMMA/GNP nanocomposite with 2 wt% GNP concentration [Color figure can be viewed at wileyonlinelibrary.com]



peaks (with the existence of GNPs at polymer structure) in literature.^{31,32}

The structural characterization indicated that GNP was integrated within the PMMA structure synthesized by the ATRP method. The polymerization process has resulted in the optimum interaction between GNP and PMMA at the PMMA/GNP nanocomposites in this study. The enhanced interfacial interaction (between GNS and PMMA matrix) was attributed to obtain the optimum fluidity and the suitable spreading of the solution has provided to avoid the fracture of GNP during the stirring processes using the suitable rotating equipment at in situ polymerization. It was assumed that GNPs filler contributed to better improvements in thermal properties on the PMMA at 2 wt% in this study as a result of the suitable interfacial interactions between GNPs and PMMA matrix.

3.1 | Gamma transmission technique

The changes in the relative gamma intensity of PMMA/GNP nanocomposite were determined as a function of the thickness by using two different gamma sources such as Cs-137 and Co-60 radioisotopes. Hence, it was possible to determine the changes in the linear attenuation coefficient (μ_l) of pure PMMA and PMMA/GNP nanocomposites at different GNP concentrations. The

changes in the relative intensity at different GNP concentrations for the Cs-137 radioisotope were analyzed with the increase of the nanocomposite thickness (in Figure 7). The theoretical mass attenuation coefficients (μ_p) were obtained from XCOM by using chemical compositions of each sample. Linear and mass attenuation coefficients against the Cs-137 radioisotope were obtained from the experimental results. The compositions of the PMMA nanocomposite samples at different GNP concentrations are presented in Table 4.

In addition, the theoretical results from WinXCOM and the experimental results by using the Cs-137 radioisotope were compared. The differences were within acceptable ranges. It was determined that the theoretical mass attenuation coefficients were slightly higher than the experimental mass attenuation coefficients (in Table 5). Experimental results of the gamma transmission properties of pure PMMA were presented (for the Co-60 radioisotope in Table 6) and the variations in the linear attenuation coefficient were examined. The changes in the relative intensity at different GNP concentrations (for the Co-60 radioisotope) have been analyzed for different thicknesses (in Figure 8). Figure 7 and Figure 8 indicated that the comparison of the gamma intensity explained the effect of GNP wt% on the protective gamma screening variations. The slopes of the changes in the relative intensity of PMMA/GNP nanocomposites are the same trend as the rise of the

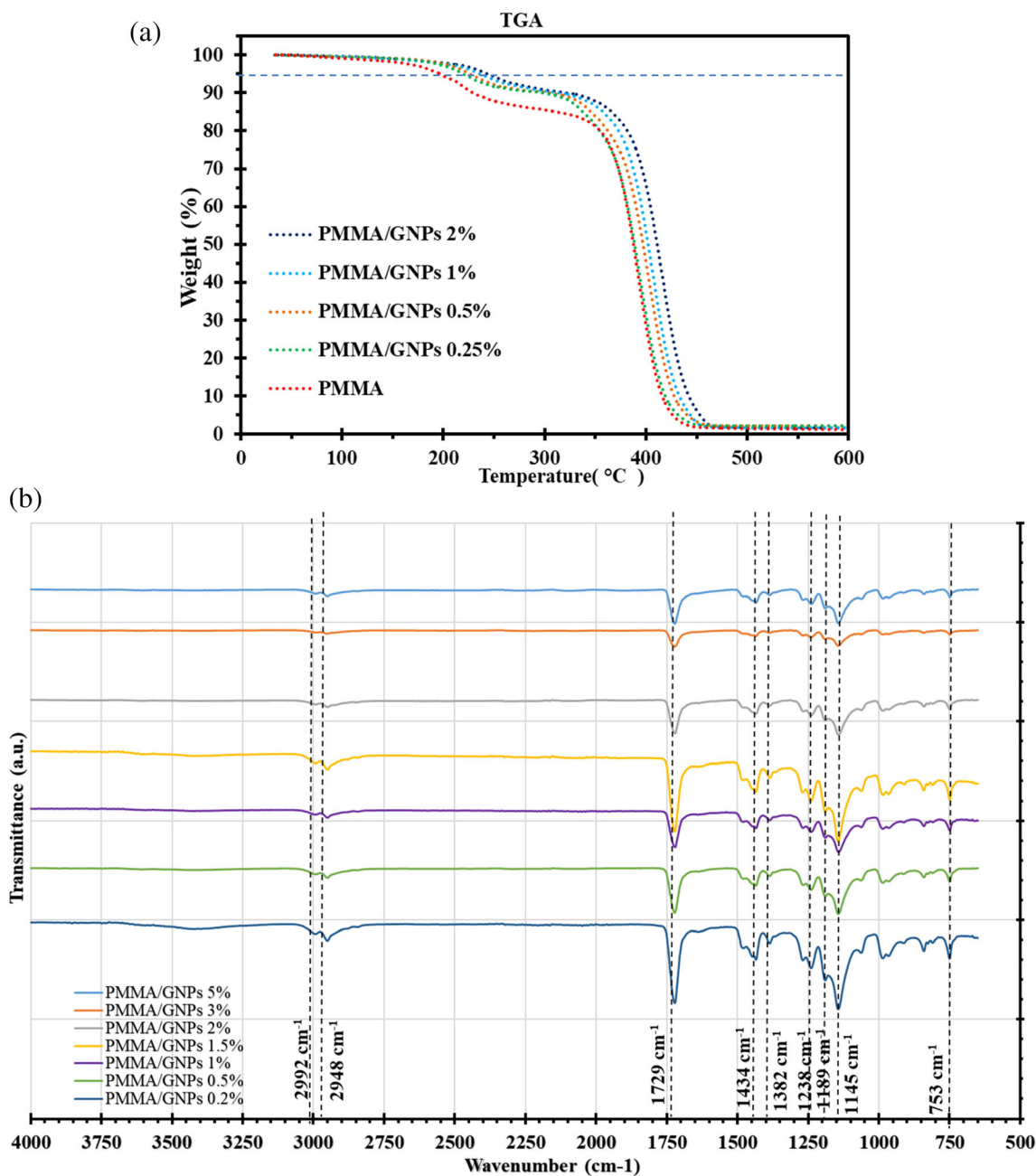


FIGURE 5 (a) TGA curves of pure PMMA and PMMA/GNPs nanocomposites. (b) FTIR analysis of the nanocomposite samples at 0.2, 0.5, 1, 1.5, 2, 3, and 5 wt% GNP amounts [Color figure can be viewed at wileyonlinelibrary.com]

TABLE 3 The changes in temperature of PMMA with the addition of GNPs at 5% weight loss

GNPs concentration in PMMA (wt%)	Temperature (at 5% weight loss of PMMA/GNPs com.) (°C)
0.00	196.73
0.25	219.33
0.50	226.03
1.00	235.87
2.00	243.00

thickness for the emitted gamma photons from Cs-137 (at 0.662 MeV) and Co-60 (at ~1.25 MeV) radioisotopes. The differences in the relative intensity were compared with the rise of the emitted gamma photon energy from the gamma sources. The highest relative intensity was identified by using Co-60 radioisotope as the transmitted photons from Co-60 radioisotope (due to its gamma photon energy) is higher than the transmitted photons from Cs-137 radioisotope (due to its gamma photon energy).

The theoretical μ_p values were obtained from WinXCOM by using the chemical compositions of each

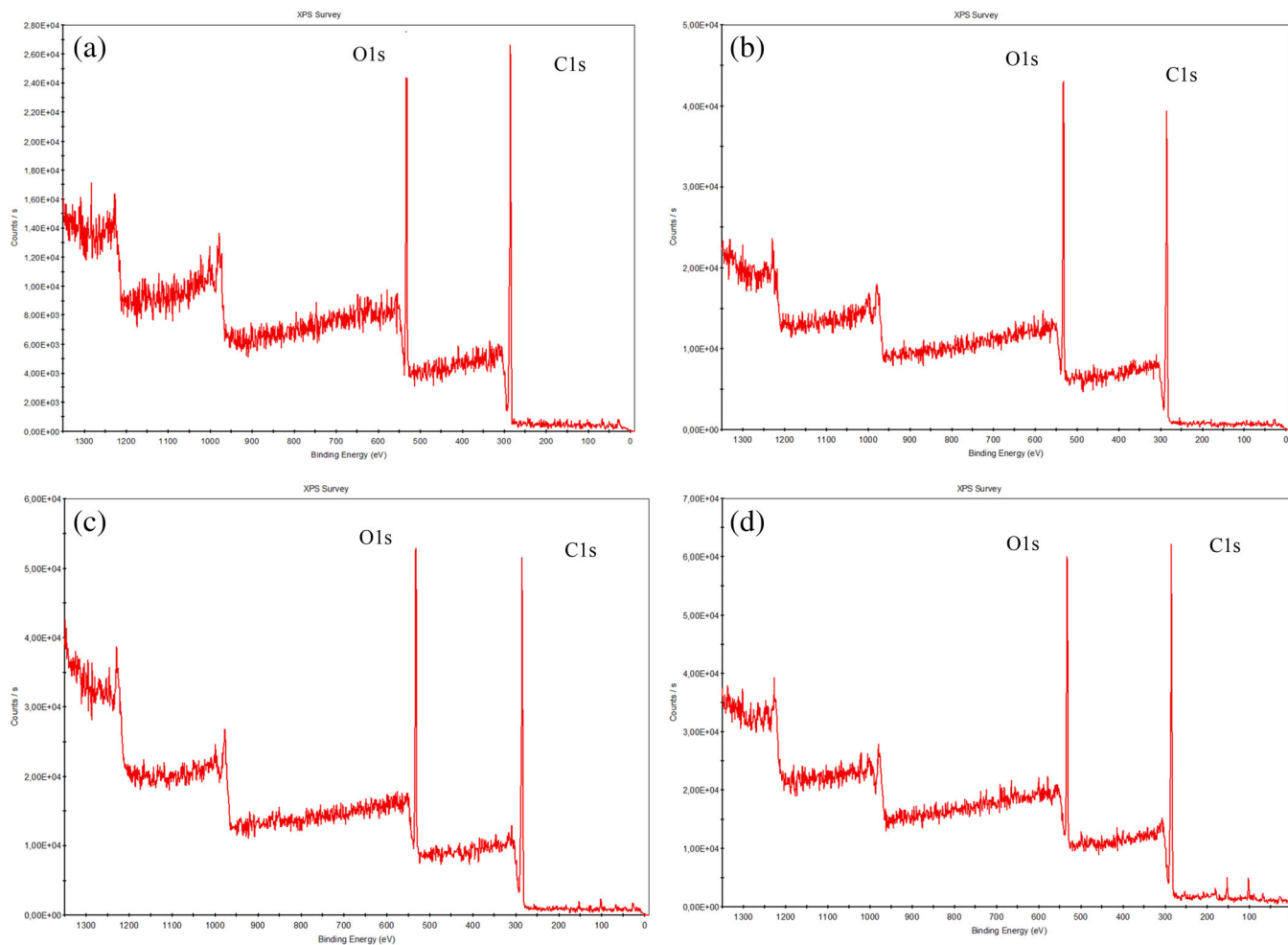


FIGURE 6 XPS survey spectrum of (a) pure PMMA, PMMA/GNP nanocomposites with (b) 0.2, (c) 1.0, (d) 2.0 wt% GNP concentration [Color figure can be viewed at wileyonlinelibrary.com]

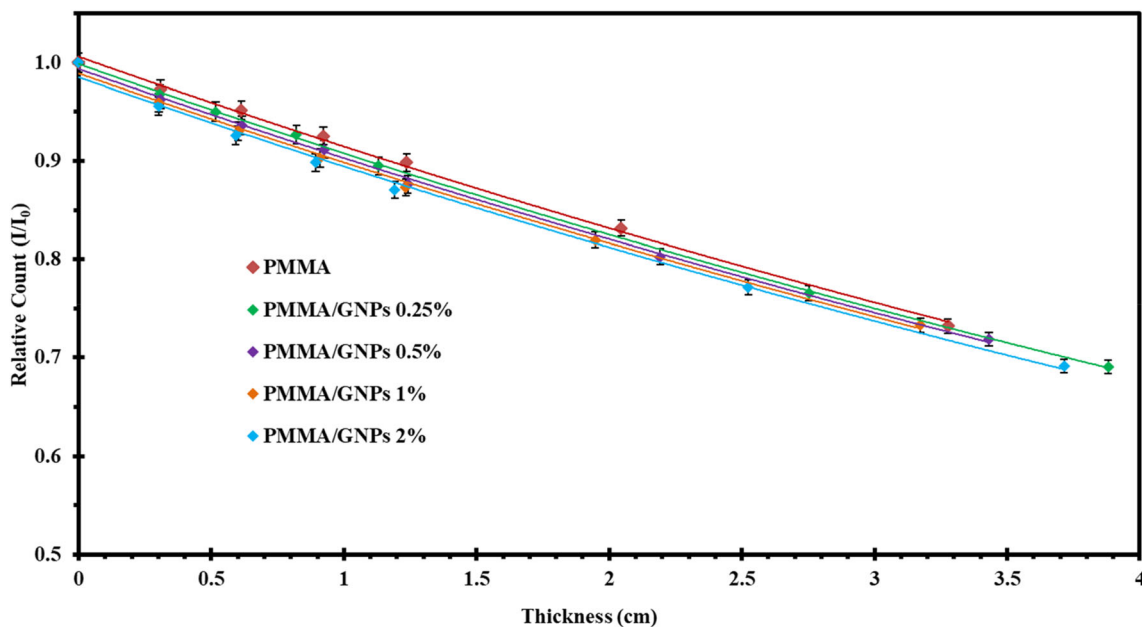


FIGURE 7 Changes in the relative intensity of PMMA/GNP nanocomposites with the rise in the thickness for Cs-137 radioisotope [Color figure can be viewed at wileyonlinelibrary.com]

Samples	C (wt%)	O (wt%)	H (wt%)	Cu (wt%)	Br (wt%)
PMMA	59.69	30.53	8.09	0.13	1.56
PMMA/GNP 0.25%	59.79	30.46	8.07	0.13	1.56
PMMA/GNP 0.5%	59.89	30.38	8.05	0.13	1.55
PMMA/GNP 1%	60.09	30.23	8.01	0.13	1.54
PMMA/GNP 2%	60.48	29.94	7.93	0.12	1.53

TABLE 4 Compositions of the PMMA nanocomposite samples with different GNP concentrations

TABLE 5 Difference between theoretical and experimental results for Cs-137 radioisotope

Samples	Linear attenuation coefficients μ (cm^{-1})	Density ρ (g/cm^3)	Mass attenuation coefficients μ/ρ (cm^2/g)	Theoretical mass attenuation coefficients (cm^2/g) (WinXCOM)	Difference (%)
PMMA	0.09521	1.18089	0.08063	0.08323	3.13
PMMA/GNP 0.25%	0.09544	1.18413	0.08060	0.08322	3.15
PMMA/GNP 0.5%	0.09569	1.18792	0.08055	0.08320	3.18
PMMA/GNP 1%	0.09601	1.19318	0.08047	0.08317	3.25
PMMA/GNP 2%	0.09668	1.20411	0.08029	0.08311	3.39

TABLE 6 Difference between theoretical and experimental results for Co-60 radioisotope

Samples	Linear attenuation coefficients μ (cm^{-1})	Density ρ (g/cm^3)	Mass attenuation coefficients μ/ρ (cm^2/g)	Theoretical mass attenuation coefficients (cm^2/g) (WinXCOM)	Difference (%)
PMMA	0.07094	1.18089	0.06007	0.06135	2.08
PMMA/GNP 0.25%	0.07108	1.18413	0.06003	0.06134	2.14
PMMA/GNP 0.50%	0.07124	1.18792	0.05997	0.06133	2.22
PMMA/GNP 1.00%	0.07142	1.19318	0.05986	0.06131	2.37
PMMA/GNP 2.00%	0.07186	1.20411	0.05968	0.06127	2.60

sample. Linear and mass attenuation coefficients against Co-60 radioisotopes were obtained from the experimental results. Linear attenuation coefficients increased with the increase in the GNP concentration. However, μ_p decreased with the increase in the GNP concentration.

The changes in the relative intensity at different GNP concentrations are analyzed in Table 5 (for Cs-137 radioisotope) and Table 6 (for Co-60 radioisotope). Hence the changes in the mass attenuations of the samples were evaluated as the compositions of the polymer nanocomposite samples at different GNP concentrations are determined in Table 4. The difference between theoretical results obtained from WinXCOM Software and the experimental results were compared by using of the gamma transmission technique. It was determined that the theoretical mass attenuation coefficient values were higher than the experimental values slightly and the differences were within acceptable ranges.

3.2 | Power coefficients

Microwave measurements from 0.01 to 110 GHz (included in X-band) for graphene integrated in low-loss microwave structures indicated that the use of graphene is essential to develop high-frequency devices.²⁷ The scattering parameter for S_{11} of a graphene transistor in the literature³³ was measured and its results presented similar values with this study. Reflection loss characteristics of a reduced graphene oxide/nitrile butadiene rubber composite with 2 wt% graphene oxide in the nitrile butadiene rubber matrix with 3 mm thickness was examined in a previous study,³⁴ and their reflection loss results presented a reflection loss level similar to that of our PMMA/GNP polymer nanocomposite with 2 wt% GNP concentration in the PMMA matrix. For the measurement of microwave parameters such as electromagnetic interference (EMI) protective gamma screening, the

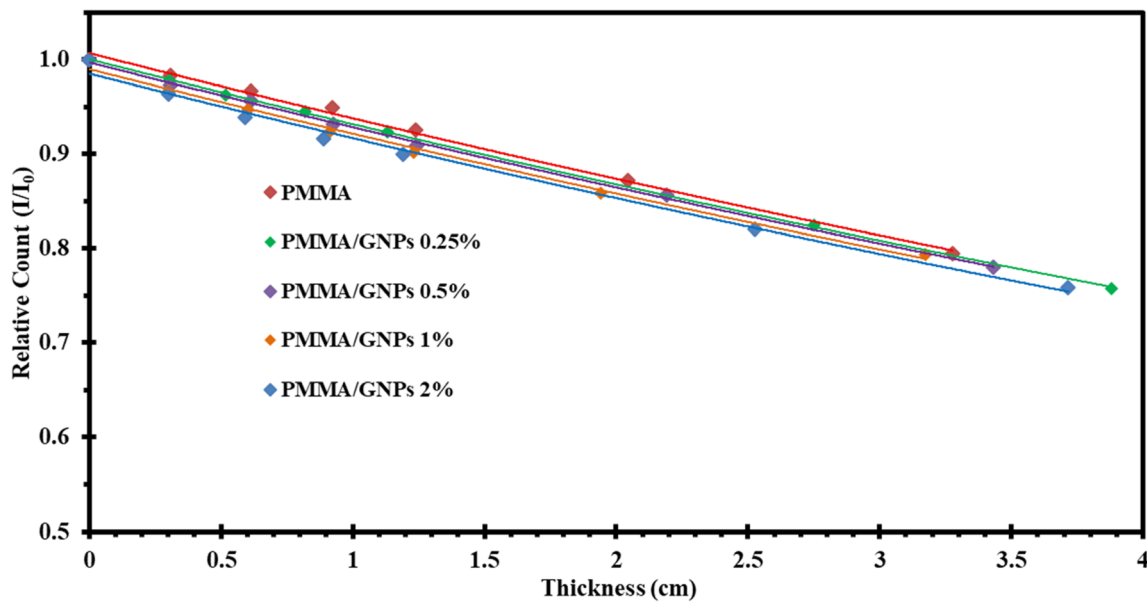


FIGURE 8 Changes in the relative intensity of PMMA/GNP nanocomposites with the rise in the thickness for Co-60 radioisotope [Color figure can be viewed at wileyonlinelibrary.com]

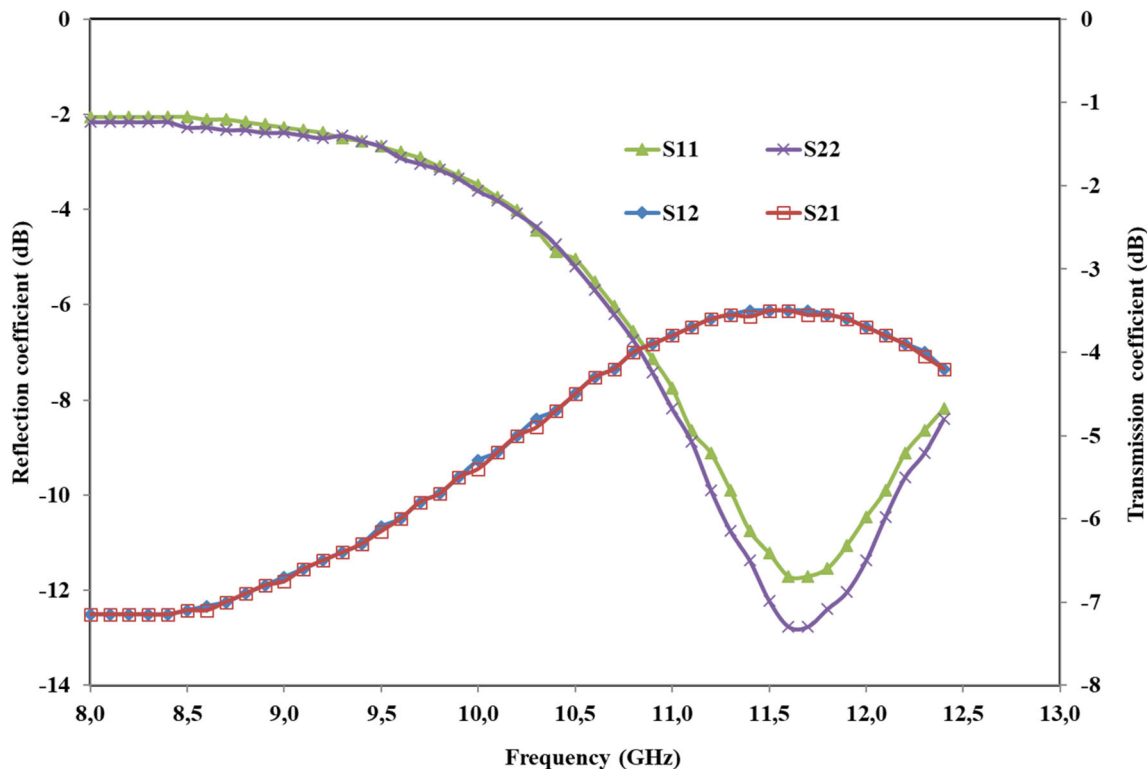


FIGURE 9 The reflection coefficients for port 1 (S_{11}) and port 2 (S_{22}) and the transmission coefficients from port 1 to port 2 (S_{21}) and port 2 to port 1 (S_{12}) [Color figure can be viewed at wileyonlinelibrary.com]

PMMA/GNP nanocomposite was placed into the aluminium shim given in Figure 2. The S-parameters (S_{11} , S_{12} , S_{21} , and S_{22}) of the nanocomposite were measured using the calibrated VNA using the waveguide method in the

X-band in this study and measured S-parameters in logarithmic scale (dB) are given in Figure 9. The measured reflection coefficients for the two ports (S_{11} and S_{22}) and transmission coefficients from the two-ways (S_{12} and S_{21})

were nearly same ($S_{11} \cong S_{22}$ and $S_{21} \cong S_{12}$) in Figure 9. The measured nanocomposite can be classified as a reciprocal material according to these results. The power coefficients such as the reflection, transmission and absorption coefficients were calculated according to Equations (1)–(3).³⁵

$$\text{Reflection, } R (\%) = 100 |S_{11}|^2 \quad (1)$$

$$\text{Transmission, } T (\%) = 100 |S_{21}|^2 \quad (2)$$

$$\text{Absorption, } A (\%) = 100 - R (\%) - T (\%) \quad (3)$$

The $T (\%)$ and $R (\%)$ parameters can also be computed using the other S- parameters such as S_{22} and S_{12} because of the reciprocal behavior of the nanocomposite material. The changes in the power coefficients such as $T (\%)$, $R (\%)$ and $A (\%)$ for the PMMA/GNP nanocomposite with 2 wt% GNP concentration are presented for the X-band frequency range in Figure 10. The reflection and transmission are changed from 7% to 62% and from 19% to 45% and averages are 36% and 32% respectively in the band. These results show that the measured material behavior is mostly reflective up to around 10 GHz. The

average and standard deviation of the absorption are 32% and 12%, respectively. The applied microwave signal to the nanocomposite material is mostly attenuated inside the measured material at the high frequencies in the band.

The measured reflection coefficient accounts for not only the reflected electromagnetic waves from the external surface, but involves the contribution of the internal surface reflection and multiple reflections.³⁵ The absorption efficiency, $AE (\%) = A/(1-R)$, shows the attenuation contribution of electromagnetic absorption including microwave (in Figure 10) when the waves travel into the materials.³⁵ Average and standard deviation for the absorption efficiency are 50% and 2% respectively for the entire frequency band. It means that the absorption efficiency has a flat response to X-band and the absorption efficiency does not depend the frequency. On the other hand, half of the applied signal is absorbed by the PMMA/GNP nanocomposites.

The total experimental shielding effectiveness (SE_{total}) which is one of another important microwave parameter to indicate relation between incident and transmitted power is the sum of the net shielding by reflection (SE_{ref}) and absorption (SE_{abs}), involving the contribution of multiple reflections, as shown in Equations (4)–(6).³⁵

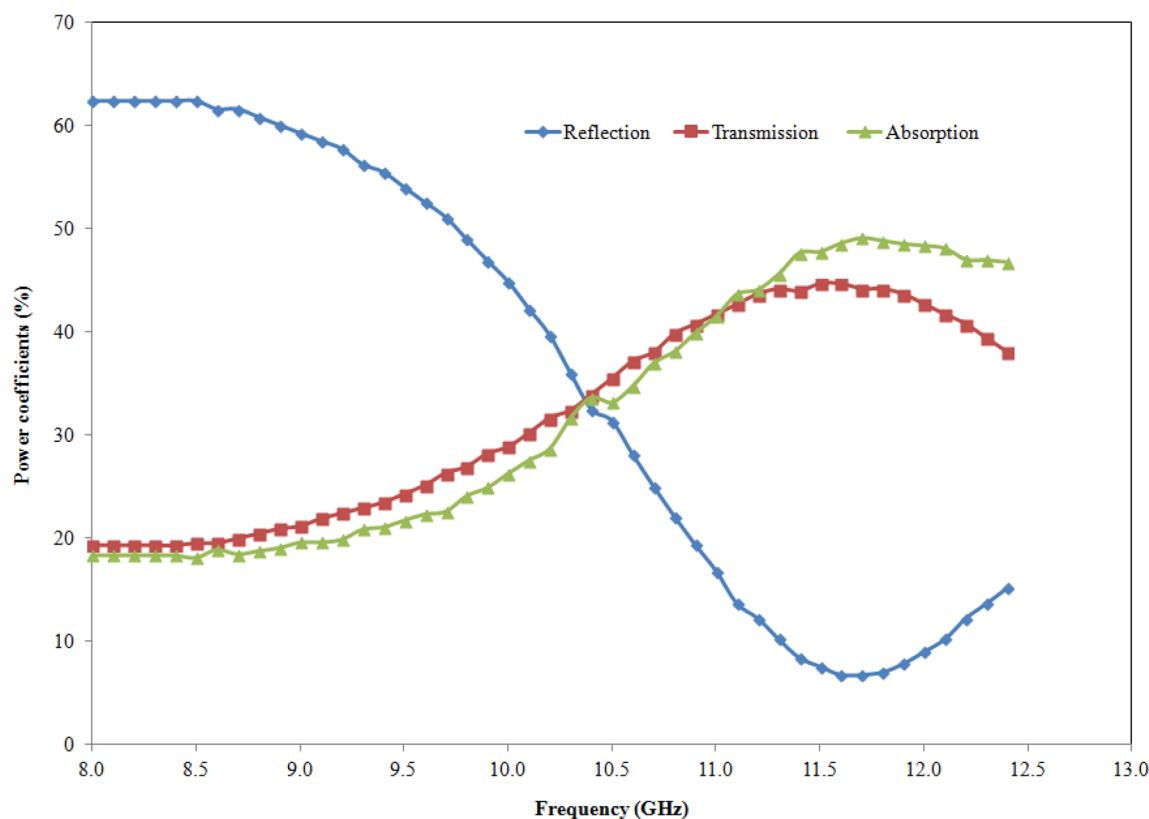


FIGURE 10 Power coefficients $T (\%)$, $R (\%)$, and $A (\%)$ of PMMA/GNP nanocomposite with 2 wt% GNP concentration [Color figure can be viewed at wileyonlinelibrary.com]

$$SE_{\text{ref}}(\text{dB}) = -10 \log(1 - R) \quad (4)$$

$$SE_{\text{abs}}(\text{dB}) = -10 \log(T/(1 - R)) \quad (5)$$

$$SE_{\text{total}}(\text{dB}) = SE_{\text{ref}}(\text{dB}) + SE_{\text{abs}}(\text{dB}) \quad (6)$$

The total electromagnetic shielding effectiveness of the PMMA/GNP nanocomposites are presented in Figure 11. The SE_{abs} has nearly same value as 3.0 dB while the SE_{ref} value is changed around 2.2 dB over the frequency range. Total value of the shielding effectiveness average is 5.2 dB with 1.4 dB standard deviation and the average is calculated 70% in linear scale for the X-band. The power coefficients and shielding effectiveness results show that the measured material can be optimized for using absorber or reflectance for X-band.

The power coefficient results (in Figure 9) presented the similar results of the thermoplastic polymer in the literature.³⁶ The electromagnetic shielding effectiveness (including R , A ; the absorption efficiency) of PMMA/MWCNT nanocomposites presents an importance in the previous study.³⁷ The PMMA/GNP nanocomposites has presented the similar characteristic changes for GNPs in Figure 11 at this study. The power coefficient (in Figure 9), the absorption efficiency (in Figure 11) and the electromagnetic shielding effectiveness (in Figure 12) derived from the scattering parameters presented similar results according to the literature.³³

The elemental mapping of the PMMA/GNP nanocomposite is important as the dispersion of Cu atoms at different C atom amount levels can affect

gamma ray absorbance in the PMMA/GNP nanocomposite. Hence, the examination of the dispersion of Cu atoms explained that there was an optimum dispersion in the PMMA/GNP nanocomposite to perform an optimum absorption for gamma rays. The examination for the dispersion of Cu atoms was performed in the composition of the PMMA/GNP nanocomposite used that can specifically absorb gamma rays in Figure 4.

GNP has lower mass density with superior thermal properties than other conventional nanofillers such as nanoclays. GNP contains several monolayer graphene with outstanding properties. The slight density improvement was determined sensitively at the PMMA/GNP nanocomposite by using the gamma transmission technique when the GNP amount increased from 0.5 to 2 wt% in PMMA synthesized by ATRP method. The results of the gamma transmission technique in Figure 7 (by using the Cs-137 radioisotope) and Figure 8 (by using the Co-60 radioisotope) indicated that the rise in the number of nanoplatelets enhanced the scattering of gamma rays slightly, and transmission of gamma ray reduced slightly. The gamma ray absorption of the samples has been affected slightly depending on the changes of the gamma attenuation (in Tables 5 and 6) by the rise in the number of graphene nanoplatelets. The increase of the gamma ray absorption indicated the slight improvement in the density. The specific effects of graphene-PMMA polymerization conditions have been monitored by gamma transmission method. Because the use of copper atoms at in-situ polymerization method have improved the gamma-ray absorption in the final polymer nanocomposite.³⁸ The copper content supported the

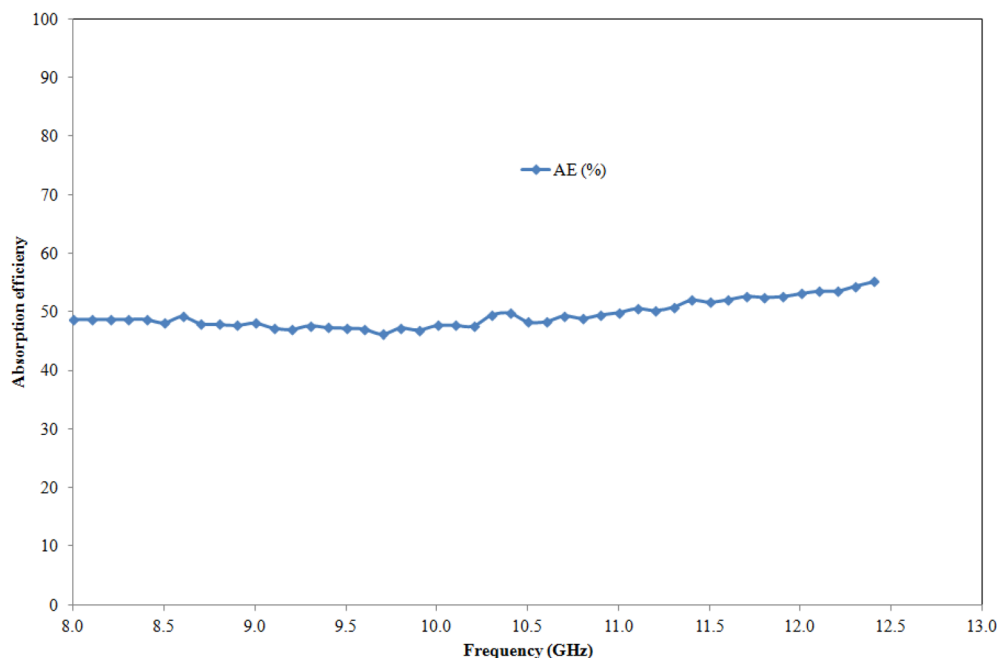


FIGURE 11 Absorption efficiency of PMMA/GNP nanocomposite with 2 wt% GNP concentration [Color figure can be viewed at wileyonlinelibrary.com]

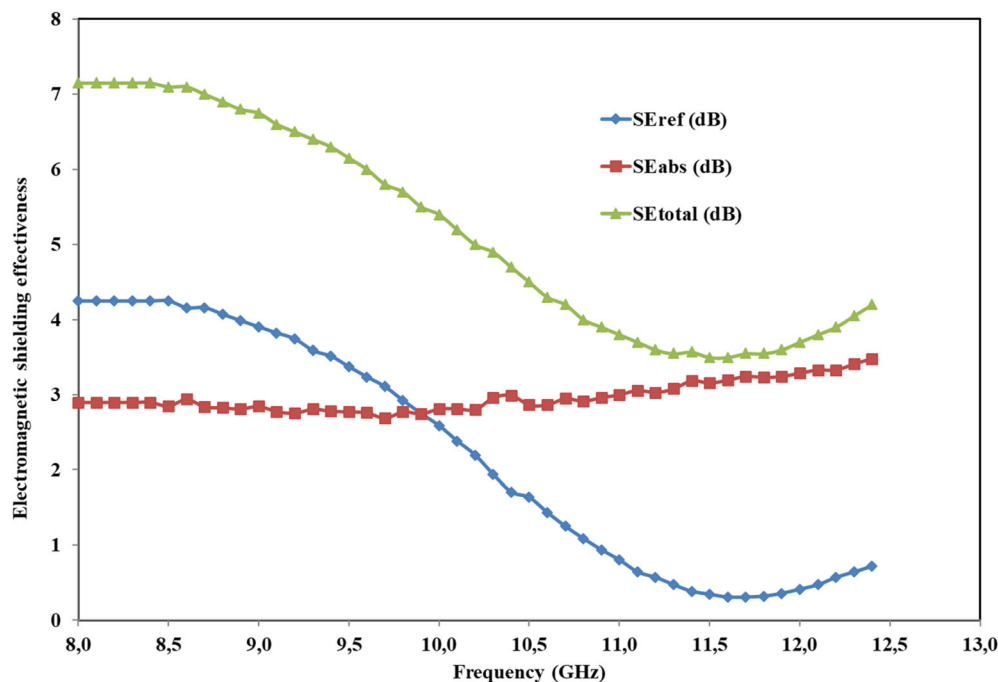


FIGURE 12 The total electromagnetic shielding effectiveness (SE) of PMMA/GNP nanocomposites 2 wt% GNP concentration [Color figure can be viewed at wileyonlinelibrary.com]

gamma absorption has not been varied in the current samples to obtain the same dispersion condition in the final polymer nanocomposite. CuBr has optimal product yields in the polymer nanocomposite structure synthesized by ATRP method.²⁹ Hence it was assumed that the physical features of the PMMA/GNP nanocomposite reinforced at 2 wt% GNP indicated that copper amount was suitable to obtain the optimum microwave absorption at X-band.

The change of GNP amount was small, but it has provided the difference on the protective gamma screening. The high R-squared value indicated the statistical measure of how close the data were to the fitted regression line for the relative intensity (I/I_0)-thickness curves of all samples. Because, the high R-squared value was determined as ~ 0.99 for all samples. The fitted line has displayed the relationship between relative intensity and thickness for real experimental data of the nanocomposite samples.

In the previous study informs that the addition of colemanite in PMMA has provided to changes the physical performance and the structural characteristics of the PMMA and the important researches have been performed on the structural properties of PMMA to support the advances in the thermoplastic engineering material based the researches in space researches of the International Space Station (ISS).²⁹ This new PMMA-based nanocomposite has assisted in understanding the relations between the protective gamma screening capacity and microwave absorption to use as potential satellite-oriented polymer materials. The structural investigations

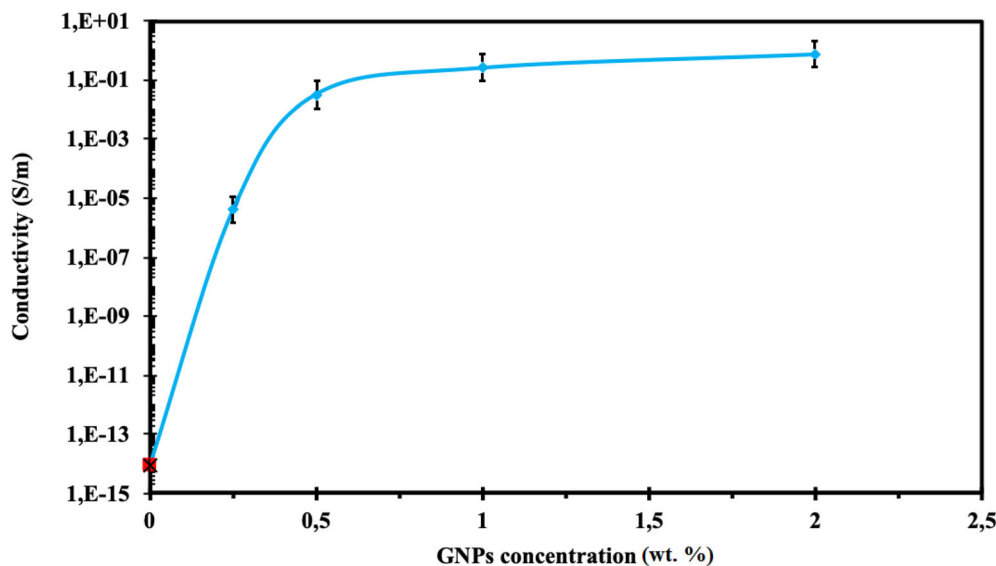
of this nanocomposite addressed to make advances for safer and longer-lasting polymer spacecraft equipment.

The vital microwave parameters in the PMMA/GNP nanocomposite at 2 wt% GNP amount indicate that the absorption of the longwave radiation (with lower energy at filtering) can provide frequency selectivity by rejecting the unwanted broadcasting or spurious signals in nanocomposite. The PMMA/GNP nanocomposite at 2 wt% GNP can be designed for its use in several systems (such as the filters) used at the components and the units (including the types such as high pass, low pass, bandpass, and notch filters). Besides, the optimum GNP amount (2 wt%) in the PMMA/GNP nanocomposite for the use of the nanocomposite at front-end modules can be employed behind the antenna in wideband phased array antenna systems with the control of the multiple scattering increase of microwaves. Hence it can be possible to achieve low noise and high-level signal immunity with the elimination of the serious absorption mechanism problems for microwave attenuation by means of tuneable range control.

3.3 | Electrical conductivity

The curve presented an improvement in electrical conductivity as a function of GNPs concentration in PMMA (in Figure 13). Electrical conductivity was measured with four-point probe method. The max. Conductivity of PMMA was obtained with the addition of 2.0 wt% GNPs

FIGURE 13 Electrical conductivity of PMMA/GNPs nanocomposite [Color figure can be viewed at wileyonlinelibrary.com]



into PMMA polymer. The optimum distribution of GNPs nanofiller in polymer presents the importance on the changes in the electrical conductivity.^{39,40} The higher electrical conductivity can be obtained with the use of the large surface area of GNPs nanoplates and outstanding conductivity of GNPs nanofillers.^{26,34,41} Besides, there are several factors that have an impact on the electrical conductivity of the polymer nanocomposites (such as processing methods and the loading concentration).^{42,43} The inserted nanolayers at the synthesis conditions had a significant influence on the improvement of the electrical properties of the nanocomposite in this study. It was suggested that the important reason of the improvement of the electrical properties was the attractive electrical conductivity properties of GNPs. Hence GNPs improved the electrical conductivity of the insulating polymer. The GNPs nanofillers can construct a conductive network with the rise to the sudden increase in the electrical conductivity of the polymer nanocomposite. It was suggested that the cross-linkable PMMA synthesized by ATRP method provided to improve the electrical conductivity as the functional groups of ATRP (as the living radical polymerization or reversible deactivation radical polymerization) was more adaptable to the multifunctional devices at the industrial applications. In situ fast polymerization can be used to improve electrical conductivity and thermal properties of GNS/PMMA nanocomposite with the suitable dispersion of GNP.^{26,30} The improvement of the thermal properties at GNS/PMMA nanocomposite can be performed with the optimum dispersion of GNP by using in situ polymerization.⁴⁴ The optimum thermal properties at GNS/PMMA nanocomposite is offered with the ideal dispersion of GNP by using solution mixing method.⁴⁵ The incorporation of functional groups in the

PMMA (synthesized by ATRP method) is achieved by using initiators (containing functional groups). The ATRP functional groups are more suitable (as a tuning method for industrial applications) as the cross-linkable PMMA can be synthesized in a controlled manner by using MMA monomers in the ATRP method.²⁹ Hence the improvement of the physical properties (with the addition of GNP at 2 wt%) indicated that the effect of crosslink density on the modification of gamma-ray and microwave adsorption properties of the nanocomposite reached an optimum level at of 2 wt% GNP. The rise of CNTs amount supports an increase in the electrical conductivity with the modification of microwave properties.^{46–48}

The previous study about the PMMA/GNP nanocomposite synthesized by the “in situ polymerization method” explains the enhancement of the elastic parameters by using GNPs for mechanical modification. Hence it is possible to obtain a suitable modification of the PMMA/GNP nanocomposite for its advanced applications compatible with the Internet of Nano Things (IoNT) systems.²⁹ Hence it was assumed that the improved interfacial interaction between GNPs provided this electrical improvement. Electromagnetic interference shielding effectiveness (for X-band) of the nanocomposites has reached maximum with the rise of the nanofiller amount at the electrical conductivity. It was suggested that the absorption efficiency and the contribution of electromagnetic absorption including microwaves (for X-band) had an optimum (in Figure 11) as the function of the electrical conductivity with the rise of GNPs amount slightly.

The non-cracked structural development has provided the thermal resistance and it was supported to rise

the gamma-ray absorption and microwave absorbability with improvement of electrical conductivity. Hence the service of this nanocomposite was possible at more aggressive working conditions. There was a relevance between gamma-ray attenuation enhancement and thermal stability development with improvement of electrical conductivity with the development of the non-crack structure in this lightweight nanocomposite synthesized by ATRP method. The determination of the slight agglomeration variations (by using gamma-ray transmission) ensured the structural discontinuity detection to enlarge the employment of this nanocomposite at wide-band phased array antenna systems including antenna applications. The agglomeration tendency and bubble inspection details are not available with the examination of the dispersion behavior sensitively by using the gamma transmission technique at the PMMA/GNP nanocomposite in the literature. The PMMA/GNPs nanocomposite synthesized by ATRP method had the obvious non-fractured surface and this structural feature provided to obtain the optimum gamma attenuation coefficient at the cost-effective radar absorbing applications for complex working conditions on the absorption of electromagnetic waves at the different ranges (for example; to develop service duties of this aerospace engineering material working near Van Allen Belts of earth, and to develop the responsibilities of this nanocomposite at the monitoring of therapy by using IoNT connected radiation oncology devices, etc.).

The rise of CNTs amount becomes the favor of an increase in the electrical conductivity with the modification of microwave properties.^{46–48} The limitation in the agglomeration tendency of GNP in PMMA (which was modified the frequency sensitivity at X-band) has provided the enhancement of electrical conductivity in this study. Besides, the limitation in the agglomeration tendency has supported to reject Bremsstrahlung radiation. The chemical composition (at 2 wt% GNP) considering the suitable electrical conductivity has indicated the decrease of the reflectance (at X-band) and the increase of the absorption of the longwave radiation with lower energy. The details in microwave parameters supported the protection of the crucial elements of the communication infrastructure dangerously unprotected commercial satellites have been provided with the determination of the structural discontinuity by using the gamma transmission technique (with Cs-137 radioisotope at 0.662 MeV and Co-60 radioisotope at ~1.25 MeV) ensured the low noise and high-level signal immunity at the PMMA/GNP nanocomposite at 2 wt% GNP. The gamma absorption of the nanocomposite was more dominant at 2 wt% GNP than at other GNP concentrations as a result of the optimum synthesis conditions.

4 | CONCLUSIONS

PMMA/GNP nanocomposite as the potential satellite-oriented polymer has been synthesized with the gamma ray resistant lightweight material which needs to grow the space industry. The implementation of heat treatment to determine critical synthesis parameters resulted with the enhancement of the gamma-ray attenuation and electrical conductivity. The development of the thermal resistance supported to rise of microwave absorbability with modification of electrical configuration as a result of the rise of electrical conductivity. The microwave absorption of the nanocomposite synthesized by living polymerization technique provided to solve the nanocomposite problems about radio frequency (RF) at X-band. The evaluation of the density changes has detailed by using the gamma transmission technique. The effect of GNP amount on density variations of the nanocomposite was evaluated by using the gamma transmission technique to perform the optimum microwave absorption. In this study, the modification of the protective gamma screening capacity indicates that the inner side of the used protective box (for the use of the modified polymer at the outside of the electronic devices at commercial satellites) will be relatively less exposed to the space radiation. The absorption efficiency of the PMMA/GNP nanocomposites was ~50% and deviation of the AE average was lower than 5% in the frequency band. Hence this nanocomposite was suitable microwave absorbing material between 8 and 12 GHz. This lightweight polymer nanocomposite has addressed to use the radar absorbing applications in the subsurface sensors and the monitoring. The indoor and outdoor environment of the box with its future widespread use can be provided with the protective screening for high frequencies in the signal generators at electrical-electronic circuit/devices. The improving gamma-ray and microwave absorption have indicated the importance of graphene-PMMA nanocomposite for its use in different electro-static and conductive applications (including critical microwave modules and microwave packaging technologies) in this study. The several devices can use the graphene-PMMA nanocomposite at relevant commercial organizations (such as space aviation industry, unmanned aerial, and marine vehicles technology).

ACKNOWLEDGMENTS

This study is supported financially by Istanbul Teknik Üniversitesi ITU BAP with the project number 41576 for the development of the new engineering samples. TUBITAK (with project no. TUBITAK1001 115R017) had supported financially a part of this study for the synthesis of the first base polymer sample researches. The

nanocomposite was synthesized at ITU Prof. Dr. Adnan Tekin of the Materials Science & Production Technologies Applied Research Center (ATARC), Istanbul, Turkey.

ORCID

Tayfun Bel  <https://orcid.org/0000-0002-0924-1893>

Mahmut Muhammettursun  <https://orcid.org/0000-0001-7906-5891>

Elif Kocacinar  <https://orcid.org/0000-0001-8772-456X>

Ecem Erman  <https://orcid.org/0000-0003-1831-7201>

Fuat Berke Gul  <https://orcid.org/0000-0001-7860-6756>

Emre Dogan  <https://orcid.org/0000-0001-5638-614X>

Murat Celep  <https://orcid.org/0000-0001-7754-4856>

Nilgun Baydogan  <https://orcid.org/0000-0001-9843-1615>

REFERENCES

- [1] R. Panwar, S. Puthucheri, V. Agarwala, D. Singh, *J. Electromagn. Waves Appl.* **2015**, *29*, 1238.
- [2] T. Bel, N. Baydogan, H. Cimenoglu, *Int. J. Mech. Produc. Eng.* **2014**, *2*, 55.
- [3] O. Olabisi, K. Adewale, *Handbook of Thermoplastics*, 2nd ed., CRC Press, Taylor and Francis Group, New York **2016**.
- [4] A. Kausar, *Polym.-Plast. Technol. Mater.* **2019**, *58*, 821.
- [5] L. Azevedo, J. L. Antonaya-Martin, P. Molinero-Mourelle, J. del Rio-Highsmith, *J. Clin. Exp. Dent.* **2019**, *11*, e670.
- [6] K. Matyjaszewski, J. Xia, *Chem. Rev.* **2001**, *101*, 2921.
- [7] K. Matyjaszewski, T. P. Davis, *Handbook of Radical Polymerization*, Wiley, New York **2003**.
- [8] S. Heunisch, L. O. Fhager, L.-E. Wernersson, *IEEE Antennas Wirel. Propag. Lett.* **2019**, *18*, 1377.
- [9] M. Aliofkhaezraei, N. Ali, W. I. Milne, C. S. Ozkan, S. Mitura, J. L. Gervasoni, *Graphene Science Handbook: Electrical and Optical Properties*, CRC Press, Taylor & Francis Group, New York **2016**.
- [10] P. Blake, P. D. Brimicombe, R. R. Nair, T. J. Booth, D. Jiang, F. Schedin, L. A. Ponomarenko, S. V. Morozov, H. F. Gleeson, E. W. Hill, A. K. Geim, K. S. Novoselov, *Nano Lett.* **2008**, *8*, 1704.
- [11] K. S. Kim, Y. Zhao, H. Jang, S. Y. Lee, J. M. Kim, K. S. Kim, J.-H. Ahn, P. Kim, J.-Y. Choi, B. H. Hong, *Nature* **2009**, *457*, 706.
- [12] W. Choi, J. Lee, *Graphene: Synthesis and Applications*, CRC Press, Taylor & Francis Group, New York **2016**.
- [13] Y. Hernandez, V. Nicolosi, M. Lotya, F. M. Blighe, Z. Sun, S. De, I. T. McGovern, B. Holland, M. Byrne, Y. K. Gun'ko, J. J. Boland, P. Niraj, G. Duesberg, S. Krishnamurthy, R. Goodhue, J. Hutchison, V. Scardaci, A. C. Ferrari, J. N. Coleman, *Nat. Nanotechnol.* **2008**, *3*, 563.
- [14] B. Li, W.-H. Zhong, *J. Mater. Sci.* **2011**, *46*, 5595.
- [15] A. Naz, A. Kausar, M. Siddiq, M. A. Choudhary, *Polym.-Plast. Technol. Eng.* **2016**, *55*, 171.
- [16] T. Bel, G. Ulku, N. Kizilcan, H. Cimenoglu, N. Yahya, N. Baydogan, *AIP Conf. Proc.* **2016**, *1787*, 050028.
- [17] R. S. Chen, M. F. H. M. Ruf, D. Shahdan, S. Ahmad, *PLoS One* **2019**, *1*, 16.
- [18] J. Ervin, M. Mariatti, S. Hamdan, *Proc. Chem.* **2016**, *19*, 897.
- [19] T. Bel, N. D. Baydogan, H. Cimenoglu, in *Effect of Curing Time on Poly(methacrylate) Living Polymer, Energy Systems and Management*, 1st ed. (Eds: A. N. Bilge, A. Ö. Toy, M. E. Günay), Springer, New York **2015**.
- [20] T. Bel, H. Cakar, N. Yahya, C. Arslan, N. Baydogan, *Defect Diffus. Forum* **2017**, *380*, 227.
- [21] S.-M. Yuen, C.-C. M. Ma, C.-L. Chiang, J.-A. Chang, S.-W. Huang, S.-C. Chen, C.-Y. Chuang, C.-C. Yang, M.-H. Wei, *Compos. A: Appl. Sci. Manuf.* **2007**, *38*, 2527.
- [22] M. Danish, S. Luo, *Sci. Rep.* **2019**, *9*, 16920.
- [23] J. E. L. de Siqueirap, J. P. Gleize, *IBRACON Struct. Mater. J.* **2020**, *13*, 455.
- [24] A. Paydayesh, A. Arefazar, A. Jalaliarani, *J. Appl. Polym. Sci.* **2016**, *133*, 1.
- [25] T. Dogan, N. Baydogan, *Int. J. Polym. Mater. Polym. Biomater.* **2020**, *69*, 831.
- [26] L. Y. Zhang, Y. F. Zhang, *J. Appl. Polym. Sci.* **2016**, *133*, 1.
- [27] H. S. Skulason, H. V. Nguyen, A. Guermoune, V. Sridharan, M. Siaj, C. Caloz, T. Szkopek, *Appl. Phys. Lett.* **2011**, *99*, 153504.
- [28] X. Yuan, L. Zou, C. Liao, J. Dai, *Exp. Polym. Lett.* **2012**, *6*, 847.
- [29] M. Muhammettursun, T. Bel, E. Kocacinar, E. Erman, F. B. Gul, A. T. Augousti, N. Baydogan, *J. Appl. Polym. Sci.* **2021**, *138*, 50689. <https://onlinelibrary.wiley.com/doi/epdf/10.1002/app.50689>.
- [30] Y. Yigit, A. Kilislioglu, S. Karakus, N. Baydogan, *J. Invest. Eng. Technol.* **2019**, *2*, 2687.
- [31] R. Sadri, M. Hosseini, S. N. Kazi, S. Bagheri, N. Zubir, G. Ahmadi, M. Dahari, T. Zaharinie, *Chem. Phys. Lett.* **2017**, *675*, 92.
- [32] Y. Geng, S. J. Wang, J.-K. Kim, *J. Colloid Interface Sci.* **2009**, *336*, 592.
- [33] Y.-M. Lin, K. A. Jenkins, A. Valdes-Garcia, J. P. Small, D. B. Farmer, P. Avouris, *Nano Lett.* **2009**, *9*, 422.
- [34] G. Chen, W. Weng, D. Wu, C. Wu, *Eur. Polym. J.* **2003**, *39*, 2329.
- [35] W.-L. Song, M.-S. Cao, M.-M. Lu, S. Bi, C.-Y. Wang, J. Liu, J. Yuan, L.-Z. Fan, *Carbon* **2014**, *66*, 67.
- [36] M. H. Moeini, M. Hossein, N. Famili, K. Foroogh, M. S. Alkhouh, N. Ghahvechian, *J. Elec. Eng.* **2014**, *14*, 32.
- [37] S. Pande, B. P. Singh, R. B. Mathur, T. L. Dhami, P. Saini, S. K. Dhawan, *Nanoscale Res. Lett.* **2009**, *4*, 327.
- [38] T. Bel, C. Arslan, N. Baydogan, *Mater. Chem. Phys.* **2019**, *221*, 58.
- [39] V. Poblete, M. Alvarez, V. Fuenzalida, *Polym. Compos.* **2009**, *30*, 328.
- [40] H. Pang, T. Chen, G. Zhang, B. Zeng, Z.-M. Li, *Mater. Lett.* **2010**, *64*, 2226.
- [41] T. Ramanathan, S. Stankovich, D. Dikin, H. Liu, H. Shen, S. Nguyen, L. Brinson, *J. Polym. Sci. Part B: Polym. Phys.* **2007**, *45*, 2097.
- [42] P. N. Khanam, D. Ponnamma, M. AL-Madeed, *Electrical Properties of Graphene Polymer Nanocomposites, Graphene-Based Polymer Nanocomposites in Electronics*, Springer, New York **2015**, p. 25.
- [43] D. Galpaya, M. Wang, M. Liu, N. Motta, E. Waclawik, C. Yan, *Graphene* **2012**, *1*, 30.

- [44] J. Wang, H. Hu, X. Wang, C. Xu, M. Zhang, X. Shang, *J. Appl. Polym. Sci.* **2011**, *122*, 1866.
- [45] G. Gonçalves, P. A. Marques, A. Barros-Timmons, I. Bdkin, M. K. Singh, N. Emami, J. Grácio, *J. Mater. Chem.* **2010**, *20*, 9927.
- [46] S. V. Kondrashov, M. Gurevich, O. V. Popkov, K. A. Shashkeev, A. S. Fionov, M. A. Soldatov, G. Yurkov, *Polym. Sci.* **2017**, *3*, 279.
- [47] S. V. Kondrashov, M. A. Soldatov, A. G. Gunyaeva, K. A. Shashkeev, O. A. Komarova, D. Y. Barinov, G. Y. Yurkov, V. G. Shevchenko, A. M. Muzafarov, *J. Appl. Polym. Sci.* **2018**, *46108*, 1.
- [48] K. A. Shashkeev, S. V. Kondrashov, O. V. Popkov, L. V. Solovianchik, M. V. Lobanov, V. S. Nagornaya, M. A. Soldatov, V. G. Shevchenko, A. I. Gulyaev, V. V. Makarova, G. Y. Yurkov, *J. Appl. Polym. Sci.* **2018**, *135*, 1.

SUPPORTING INFORMATION

Additional supporting information may be found online in the Supporting Information section at the end of this article.

How to cite this article: Bel T, Muhammettursun M, Kocacinar E, et al. Improvement of thermal stability and gamma-ray absorption in microwave absorbable poly(methyl methacrylate)/graphene nanoplatelets nanocomposite. *J Appl Polym Sci.* 2021;138:e50897. <https://doi.org/10.1002/app.50897>